

Multiplexed Free-Standing Nanowire Transistor Bioprobe for Intracellular Recording: A General Fabrication Strategy

Lin Xu,^{†,‡,⊥} Zhe Jiang,^{†,⊥} Liqiang Mai,[‡] and Quan Qing^{*,§,||}

[†]Department of Chemistry and Chemical Biology, Harvard University, Cambridge, Massachusetts 02138, United States

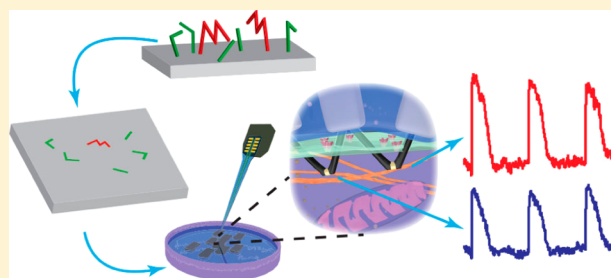
[‡]State Key Laboratory of Advanced Technology for Materials Synthesis and Processing, WUT-Harvard Joint Nano Key Laboratory, Wuhan University of Technology, Wuhan 430070, China

[§]Department of Physics and ^{||}Biodesign Institute, Arizona State University, Tempe, Arizona 85287, United States

S Supporting Information

ABSTRACT: Recent advance in free-standing nanowire transistor bioprobes opens up new opportunities of accurately interfacing spatially unobstructed nanoscale sensors with live cells. However, the existing fabrication procedures face efficiency and yield limitations when working with more complex nanoscale building blocks to integrate, for example, multiplexed recordings or additional functionalities. To date, only single-kinked silicon nanowires have been successfully used in such probes. Here we establish a general fabrication strategy to mitigate such limitations with which synthetically designed complex nanoscale building blocks can be readily used without causing significant penalty in yield or fabrication time, and the geometry of the probe can be freely optimized based on the orientation and structure of the building blocks. Using this new fabrication framework, we demonstrate the first multiplexed free-standing bioprobe based on w-shaped silicon kinked nanowires that are synthetically integrated with two nanoscale field-effect transistor devices. Simultaneous recording of intracellular action potentials from both devices have been obtained of a single spontaneously beating cardiomyocyte.

KEYWORDS: Silicon nanowire, nanoprobe, nanosensor, field-effect transistor



Recording intracellular signals from live cells plays a fundamental role in the study of cell physiology and networks.^{1–4} Conventional patch clamp technique is considered as the standard method for intracellular recording,⁵ while it faces several challenges in practice, including the difficulty in multiplexed recording, only one-time use of each pipet electrode, and ion exchange problem between recording medium and cell cytoplasm.^{5,6} Many new approaches utilizing micro/nanofabrication and nanoelectronic sensors have emerged to address these limitations, including micro/nanoscale metal pillar arrays,^{7–9} nanowire transistor based devices,^{10,11} and nanotube based sensors.^{12,13} Although these studies have highlighted the unique interactions between the nanoscale devices/structures and live cells, as well as the capability of multiplexed recording, all designs were based on devices on top of two-dimensional (2D) substrates and therefore could not allow accurately targeted recording from selected cells. In order to take full advantage of the nanoscale detectors and, importantly, to allow accurate manipulation and targeting just like working with a patch clamp pipet electrode, free-standing nanowire transistor probes have recently been developed, where a single suspended silicon kinked nanowire (KNW) transistor is positioned at the very end of a probe shaft that provides robust electrical and mechanical connection from the nanoscale device to a macroscopic printed circuit board (PCB) connector.¹⁴ The whole probe can be readily

manipulated in three-dimensions (3D) and record intracellular signals with submicrometer spatial resolution. Such a flexible design could significantly expand the application of nanoelectronic sensors in electrophysiological studies. However, the previously proposed fabrication scheme still faces several limitations in terms of efficiency and yield to work with complex nanoscale building blocks, as discussed below, and therefore a more general fabrication approach needs to be developed to enable practical construction of functional free-standing nanoelectronic probes with more complex structures, for example, to deliver multiple devices with a single probe for multiplexed recording or to integrate stimulation capability for bidirectional communication with the cells. Here we use the w-shaped Si KNW as an example to demonstrate a new fabrication framework with which the synthetically designed complex nanostructures can be effectively integrated in a free-standing probe structure for multiplexed intracellular recording.

There are three key stages in the process of building the free-standing probe starting from synthesized nanoscale building blocks, as illustrated in Figure 1: (1) Bottom-up design and synthetic preparation of functional nanomaterials on a growth substrate. (2) Transfer of nanomaterials from the growth

Received: April 7, 2014

Published: May 16, 2014

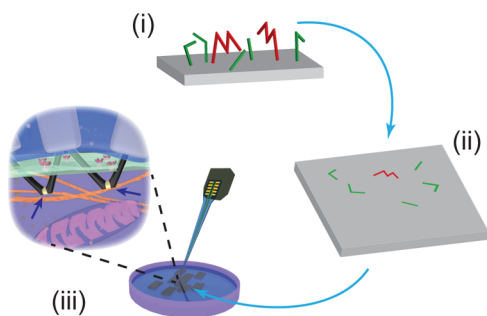


Figure 1. Key stages of fabricating free-standing nanoelectronic probes, using w-shaped Si KNW as an example. Stage (i): Design and synthesis of functional nanomaterials as nanoscale building blocks (red). The byproduct during synthesis is colored in green. Stage (ii): Transfer the nanomaterials onto the fabrication substrate and identify the one building block with desired characteristics and orientation (red), followed by fabrication of probe body by top-down lithography. Stage (iii): Release of the probe body from the substrate and assembly into a free-standing probe for accurately targeted measurements.

substrate to the fabrication substrate so that a “good” building block with the consistent structure as designed (marked in red) can be identified in designated area, followed by fabrication of the connections and probe body. (3) Full release of the probe structure from the fabrication substrate and assembly of the final free-standing probe. The main challenge in the previous approach, especially when complex nanomaterial building blocks are involved, is the low efficiency and yield in stage 2, in which the proper building blocks of ideal shape and orientation have to be identified among randomly distributed nanomaterials after the solution-based transfer step.¹⁴ Specifically, two main factors determine the feasibility of the fabrication: (1) The yield of synthesis of the building blocks usually decreases significantly as the complexity of the structure increases. For example, the growth of Si nanowires with a single 120° kink can achieve a yield of $>60\%$, while the synthesis of w-shaped KNWs, which relies on the formation of three equally spaced kinks in trans-orientations, has a typical yield of only $\sim 10\%$.¹⁵ (2) Previously, the orientation of the main probe body is lithographically predefined on the fabrication substrate, so that only the building blocks that are in good alignment with such orientation can be used, resulting in a selection yield of $\sim 17\%$.¹⁶ Therefore, the combined yield of finding a matching structure in the post-transfer selection step can be significantly poorer ($<2\%$ for the w-shaped KNWs) and the overall fabrication design becomes impractical for working with complex building blocks with low yield in synthesis. Here, we propose a new fabrication strategy in which the orientation and position of the probe structure are determined only by the selected building block with the desired structure, rather than by predefined lithography. The removal of the orientation and position constraint in the selection step maximizes the efficiency of the fabrication process and makes it possible to further improve the yield by pure optimization of the synthesis process.

The construction of free-standing multiplexed bioprobes is used to demonstrate our new fabrication strategy. The integration of multiple devices on a single probe can increase the efficiency and spatial resolution of recording. In addition, it can enable identifying the position of signal sources by triangulation for implanted recordings from a large population of neurons.¹⁷ However, the assembly of multiple single-kinked

nanowires with accurate distance and orientation control is not yet possible for existing assembling techniques, which cannot maintain the integrity and shape of the KNWs due to the mechanical stress and/or shear force required for the aligning process.^{20,21} Here, we directly construct the building blocks for multiplexed Si KNW probes using gold-nanoparticle (Au-NP) catalyzed vapor–liquid–solid (VLS) growth method with precise dopant and geometric control similar to previously reported.^{15,18,19} The schematic of the w-shaped Si KNW building blocks used here is shown in Figure 2a. Specifically,

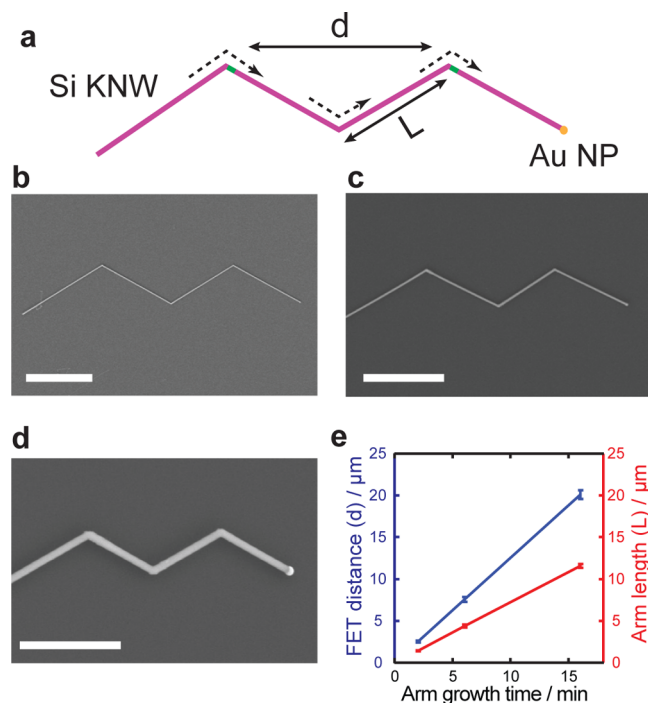


Figure 2. Accurate synthetic control of w-shaped silicon KNWs with multiplexed nanoFETs. (a) Schematic of the synthetic design of w-shaped silicon KNW. The dotted arrows denote the growth direction; the green sections mark the position of the nanoFETs. The arm length between adjacent kinks (L) and distance between nanoFETs (d) are controlled by arm growth time and the kink angles. (b–d) SEM images of KNWs synthesized using 150 nm Au-NPs as catalysts with different arm growth times of 16, 6, and 2 min, respectively. Scale bars: (b) $10\ \mu\text{m}$, (c) $5\ \mu\text{m}$, and (d) $2\ \mu\text{m}$. (e) Plots of nanoFET distance (d) and arm length (L) versus arm growth time ($n = 20$).

two nanoscale field-effect transistors (nanoFETs) are synthetically integrated at the elbows (marked in green) of the silicon nanowire with three kinks in trans-orientations. The distance d between the two nanoFETs can be accurately adjusted by controlling the growth time of the nanowire arm L between adjacent kinks. The scanning electron microscope (SEM) images of three typical w-shaped Si KNWs with different nanoFET distances are shown in Figure 2b–d with arm growth time of 16, 6, and 2 min, and arm length of 11.60, 4.40, and $1.45\ \mu\text{m}$, respectively. The dependence of arm length and FET distance on the arm growth time is plotted in Figure 2e, giving linear coefficients of 0.73 ± 0.03 and $1.26 \pm 0.08\ \mu\text{m}/\text{min}$, respectively ($n = 20$). The minimal distance between the nanoFETs can be controlled as close as $2.5\ \mu\text{m}$ with the angle of each elbow fixed at 120° . Even smaller nanoFET distance can be obtained if 60° kinks are synthesized for each elbow by

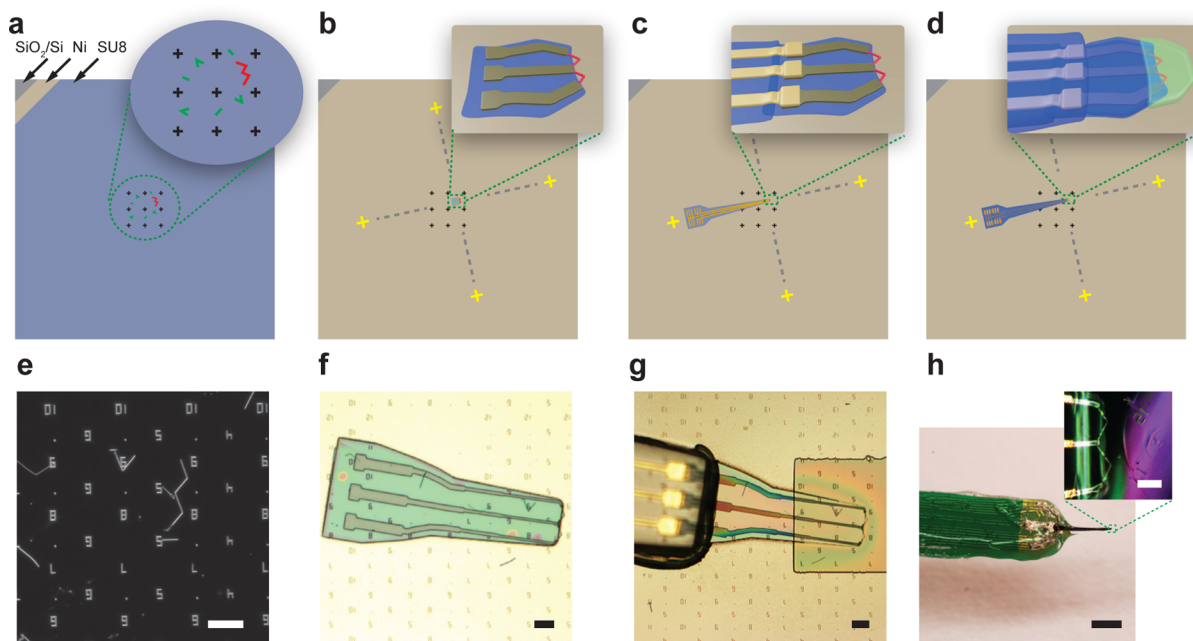


Figure 3. Key steps of fabricating free-standing probes with selected w-shaped Si KNW. (a) Si substrate with 600 nm SiO₂ and metal markers (black crosses) coated with Ni sacrificial layer and SU8 polymer layer, where silicon KNWs were deposited on the top. Inset: Magnified position marker area, where one w-shaped Si KNW with desired characteristics was selected (red) among the byproducts and nanowires that did not have the proper geometry (green). (b) The head piece fabricated by EBL steps around the selected Si KNW (inset), which included the bottom SU8 layer (blue) and metal contacts (brown, 1.5 nm Cr/120 nm Pd/60 nm Cr). A set of alignment markers (yellow crosses) were defined by additional aligned PL steps to precisely designate the position and orientation of the head piece (dotted gray lines). (c) The bottom SU8 layer (blue) of the main probe body and metal connections (golden, 5 nm Cr/200 nm Au) from the head piece to the macroscopic bonding pads were fabricated by PL using the new alignment markers. (d) Top passivation layers over the head piece and the main probe body (blue) were fabricated by EBL and PL steps. The nanowire was then protected by a photosensitive protection cap (inset, green). (e) Dark-field optical image showing a selected w-shaped Si KNW on top of the SU8 layer. The metal position markers are below the SU8 layer for the registration of subsequent lithography steps. Scale bar: 20 μm . (f) Bright-field optical image of the head piece that highlights the Si KNW at the tip, the bottom SU8 passivation layer, and the metal contacts. Scale bar: 20 μm . (g) Bright-field optical image of the probe tip with the top passivation layers and the photoresist cap over the nanowire device. The top passivation layer of the main probe body is over 50 μm thick (vs 2 μm for the head piece) to provide stronger mechanical strength and therefore it is out of focus in the image. Scale bar: 20 μm . (h) Digital camera image of a fully assembled probe on the PCB connector. The metal pins at the other end of the connector are not shown. Scale bar: 2 mm. Inset: Dark-field optical image of the suspending Si KNW nanoFET embedded in the photoresist protection cap at the tip of the probe. Scale bar: 10 μm .

combining two 120° cis-kinks sequentially at the expense of yield.¹⁵

The four key steps of fabricating free-standing multiplexed nanowire transistor bioprobes using w-shaped KNWs are illustrated in Figure 3. First, the fabrication substrate (Si with 600 nm SiO₂) with metal position markers defined by electron-beam lithography (EBL) (5 nm Cr/45 nm Au, Figure 3a, black crosses) was coated with a Ni sacrificial layer and an unexposed SU8 polymer layer. The w-shaped KNWs on the growth substrate were then dispersed in ethanol by ultrasonication and transferred to the marker area using a micropipet (Figure 3a). Once a single nanowire building block with the ideal shape as designed could be identified by a dark-field optical microscope (in red, Figure 3a, inset), its location was then registered using the position markers (Figure 3a). An example dark-field image of a selected w-shaped KNW among the position markers is shown in Figure 3e.

Second, based on the position and orientation of the selected w-shaped KNW, a microscale head piece and a new set of alignment markers were fabricated before the construction of the main probe structure (Figure 3b). Specifically, the SU8 layer adjacent to the arms of the nanowire was exposed by EBL to shape the bottom passivation layer with a typical dimension of 200 μm long by 50 μm wide, followed by additional EBL and metallization process to fabricate source/drain metal electrodes

(1.5 nm Cr/120 nm Pd/60 nm Cr) on top (Figure 3b inset). The contacts and the bottom passivation layer constituted the head piece, designating the position and orientation of the nanowire building block, as well as forming the initial contacts with the silicon nanowire. The optical image of a finished head piece is shown in Figure 3f, highlighting the w-shaped KNW at the tip of the piece, and the three contact electrodes on top of the SU8 passivation layer. In addition, four outer markers were then fabricated by photolithography (PL) (Figure 3b, yellow crosses). The center and orientation of the markers were aligned with the head piece through an observation window on the photo mask, as indicated by the gray dotted line in Figure 3b.¹⁹ Third, the bottom SU8 passivation layer for the main probe structure, which linked with the existing head piece, was fabricated by PL based on the new set of alignment markers, followed by the PL fabrication of the metal connections that scaled from the existing metal contacts on the head piece to the millimeter-scale bonding area (Figure 3c). Last, top SU8 passivation layers with low internal stress²² of 2 and 50 μm thickness were coated over the head piece by EBL and the main probe structure by PL, respectively, using protocols as previously described.^{14,19,22} In addition, a photosensitive protection cap (Figure 3d, inset, marked in green) was fabricated around the tip of the probe, similarly to the previous design, to protect the nanowire from the capillary force in the

assembly procedures and to keep it free of contaminations before use in the recording experiments.^{14,19}

We follow the same procedure as in the previous report¹⁴ to complete the final probe for recording.¹⁹ Briefly, the whole probe-end on the fabrication substrate was fully released by chemically etching the Ni sacrificial layer and then glued onto a PCB connector with a silicon microlever, which is shorter than the nanowire/SU8 probe structure to serve as the back support. The nanowire devices were connected to the PCB using silver epoxy and the surface of the connections was coated with silicone for insulation. The picture of a fully assembled probe is shown in Figure 3h, which highlights the electrical contacts, the microlever support beneath the SU8 probe structure, the probe-end on the top, and the silicone insulation. The inset micrograph of Figure 3h shows the magnified area of the tip of the probe-end, where the suspending w-shaped KNW is embedded in the protection cap with one common source contact at the center and two drain contacts on the side arms.

Compared with the previous fabrication strategy, several unique features here should be highlighted. First, the position and orientation of the main probe structure can now be determined after the nanowire building block has been identified, whereas in previous studies¹⁴ the pattern was predefined on the fabrication substrate. Therefore, the new selection process is not restricted to a small range of positions and orientations of nanowires on the fabrication substrate. This dramatically increases the yield and efficiency of the transfer and selection process and minimizes the waste of nanowire samples, because as long as a single one nanowire building block with the ideal shape can be identified, the fabrication can proceed to the next step. For example, in the current design we can work with any nanowires within an area of ~ 1.6 mm by 1.6 mm labeled by the position marker, while previously only about a quarter of the $800 \mu\text{m}$ by $800 \mu\text{m}$ marker area can be effectively utilized with additional orientation restrictions. The overall time needed for the transfer/selection process for each chip has been significantly reduced from several hours to 20–30 min. In addition, previously the tip geometry and structure around the nanowire usually needed unfavorable adjustment from the ideal design to compensate the deviation from the required orientation and/or position; the new strategy can guarantee that the tip structure for every fabricated probe is always optimized based on the exact status of the selected nanowire, because the head piece is prepared by EBL with complete freedom of its shape, orientation and structure, before the aligned PL fabrication of the rest of the probe-end. In other words, for working with different building blocks of more complicated natures this new fabrication framework can be easily adapted for satisfying the specific needs for the probe without sacrificing the throughput of the process.

In addition, we have demonstrated the first multiplexed intracellular recording from the same cardiomyocyte cell using a single w-shaped KNW bioprobe. Specifically, the dual-nanoFET probe was mounted on a micromanipulator with a typical 60° angle from the horizontal plane for accurate positioning in 3D space. The UV-sensitive protection cap was first exposed in UV light and dissolved in MF-CD-26 (MicroChem) to reveal the fresh surface of the nanowire device, followed by coating of the nanowire with phospholipid bilayers, using similar preparation procedures as previously described.^{14,19} The recording experiment was then conducted in HEPES-based buffered recording medium with temperature regulated at 35°C .¹⁹ Before introducing the cells, the

sensitivities of both nanoFETs were obtained by the water gate measurement. Briefly, a 0.1 V bias was applied on the common source electrode at the center with the drain electrodes at both sides connected to ground through two current preamplifiers with a sensitivity of 10^6 V/A. The conductance of both devices was monitored as the chemical potential of the recording medium was changed from -0.1 V to $+0.1$ V using a Ag/AgCl as the reference electrode. The typical results are shown in Figure 4a from which we can calculate the sensitivity of the nanoFETs as $10.8 \mu\text{S/V}$ (red) and $19.2 \mu\text{S/V}$ (blue), respectively. These results are consistent with the performance of the planar devices fabricated using the w-shaped nanowires synthesized with the same protocol.¹⁵ The sensitivity data can then be used to convert the change of

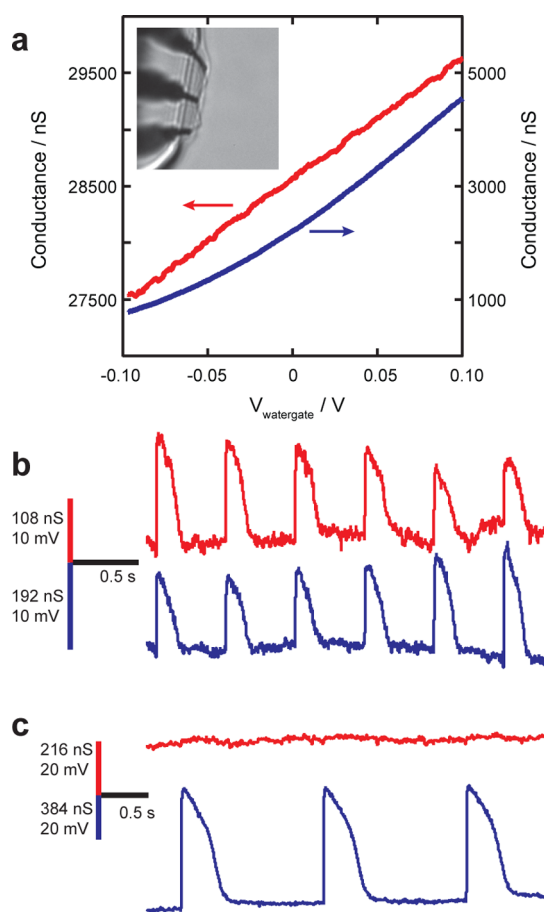


Figure 4. Multiplexed intracellular recording using the free-standing dual-nanoFET probe. (a) Conductance versus water-gate data for a typical free-standing dual-nanoFET probe after removing the photo-resist protection cap and coating with phospholipid bilayer with source/drain voltage of 0.1 V. Inset: Bright-field optical image of the probe in recording solution using an inverted microscope. The probe was mounted on the micromanipulator with a 60° angle from the horizontal plane. The suspending arms of the nanowire in the inset image appear shorter than their actual length due to the steep angle of the probe. (b) Data recorded simultaneously from both nanoFETs in contact with the same spontaneously beating cardiomyocyte. Both devices showed signals with intracellular characteristics. (c) Data recorded simultaneously from both nanoFETs while one nanoFET was in better contact with the spontaneously beating cardiomyocyte and leaving the other nanoFET deviating slightly from the cell. Only the nanoFET device in contact with the cell showed strong intracellular signal (blue).

conductance of each device to the potential change at the surface of each nanoFET.

Spontaneously beating cardiomyocyte cells cultured on a thin PDMS substrate were then introduced to the recording chamber on the inverted microscope; the probe was positioned close to a selected cell using the micromanipulator with submicrometer accuracy in the x - y plane (limited by imaging quality) and brought down to form gentle contacts with the cell with 40 nm step size in the z -distance. We have typically observed the devices picking up signals with intracellular action potential (APs) characteristics^{23,24} within 20 s after the contact was formed. Representative traces from both devices are shown in Figure 4b, which gives simultaneously recorded signals from both nanoFETs with amplitudes of 14 ± 2 and 10 ± 2 mV and durations of 133 ± 6 and 129 ± 6 ms, respectively ($n = 6$). We note that the amplitudes of both signals were smaller and less stable than the typical values of APs recorded using one single-kinked nanoFET bioprobe,¹⁴ and there were small variations in amplitudes and shapes between the signals from the two devices, although all signals were tightly synchronized by the fast rising edge ($\Delta t < 10 \mu\text{s}$). This indicates that the devices were not yet at the optimal position inside the cell for intracellular recording, and the sealing of the devices at the cell membrane was not stable. In order to further clarify these discrepancies, a control experiment was designed in which we tuned the lateral mounting angle of the probe on the manipulator $\sim 30^\circ$ toward the side arm of the w-shaped nanowire which has one nanoFET on it (see the schematic in Figure 2a showing a green nanoFET section on the right side arm of the W-shaped nanowire). As a result, the nanoFET on the side arm should form a better contact with the cell with a shallower access angle, while leaving the other device deviating slightly from the cell. As shown in Figure 4c, only the device in contact with the cell gave pronounced intracellular AP signals (blue trace) with amplitude of 52 ± 3 mV and duration of 129 ± 2 ms, which were consistent with previous reports,^{10,14} while the other device was silent (red trace). Therefore, we tentatively attribute the nonideal quality of the signals recorded with dual-nanoFETs from a single cell to the geometric limitations of the device in the current synthetic design. Namely, the channel length of the nanoFETs is ~ 500 nm, and the extending length of the nanowire from the edge of the SU8 passivation layer at the tip of the probe is $1\text{--}2 \mu\text{m}$. When the devices were set with an angle to touch the cell together, both nanoFETs have to travel >250 nm from the cell surface to gain full access to the cytoplasm due to the 120° opening angles of the kinks. Furthermore, in practice, the error in nanowire arm length and misalignment in the orientation of the devices could require even longer travel distance to gain full intracellular signals from both devices, which makes the position control quite difficult to avoid damage to the cell and obtain stable recordings. Consequently, when we obtained reasonable level of signals from both devices before hurting the cell, the nanoFETs were most likely not fully inside cell yet, resulting in weaker signals. In addition, the relatively large 120° angles between the nanowire arms here compared to previously 60° angle in the case of a single-kinked probe and the close distance ($<10 \mu\text{m}$) between the devices led to larger cross section when both devices entered the cell and had a higher probability of damage and leakage, which could also degrade the quality of signal. Nevertheless, we also note that the geometry of the probes could be optimized by a more elaborate synthetic design to address the existing issues by incorporating ultrasmall U-

shaped KNW structures and further reducing the diameter of the nanowire.¹⁵ Importantly, the fabrication framework demonstrated here could still be applied without modification to the preparation of bioprobes based on the more complex nanowire building blocks.

In conclusion, we have demonstrated the first free-standing dual-nanoFET bioprobe based on w-shaped KNWs and successfully obtained the first multiplexed intracellular recording from the same cell using a single probe. Our new fabrication procedures have mitigated the yield and efficiency limitations in previous fabrication procedures and can be used as a general framework for preparation of free-standing bioprobes with optimal geometry based on any complex bottom-up designed nanoelectronic materials, opening up new opportunities in integrating additional functionalities and performance in free-standing nanoelectronic bioprobes by innovative synthetic designs of nanoscale building blocks.

■ ASSOCIATED CONTENT

Supporting Information

Materials and methods and additional references. This material is available free of charge via the Internet at <http://pubs.acs.org>.

■ AUTHOR INFORMATION

Corresponding Author

*E-mail: Quan.Qing@asu.edu.

Author Contributions

[†]L.X. and Z.J. contributed equally to this work.

Notes

The authors declare no competing financial interest.

■ ACKNOWLEDGMENTS

This work was partially supported by the National Basic Research Program of China (2013CB934103), and International Science and Technology Corporation Program of China (2013DFA50840). We express our deep thanks to Professor C. M. Lieber of Harvard University for his careful supervision, strong support, and stimulating discussion.

■ REFERENCES

- (1) Parpura, V. *Nat. Nanotechnol.* **2012**, *7*, 143–145.
- (2) Spira, M.; Hai, A. *Nat. Nanotechnol.* **2013**, *8*, 83–94.
- (3) Duan, X.; Fu, T.-M.; Liu, J.; Lieber, C. M. *Nano Today* **2013**, *8*, 351–373.
- (4) Dunlop, J.; Bowlby, M.; Peri, R.; Vasilyev, D.; Arias, R. *Nat. Rev. Drug Discovery* **2008**, *7*, 358–368.
- (5) Molleman, A. *Patch Clamping: An Introductory Guide to Patch Clamp Electrophysiology*; Wiley: New York, 2003.
- (6) Sakmann, B.; Neher, E. *Single-Channel Recording*; Plenum Press: New York, 1995; Chapter 2.
- (7) Xie, C.; Lin, Z.; Hanson, L.; Cui, Y.; Cui, B. *Nat. Nanotechnol.* **2012**, *7*, 185–190.
- (8) Robinson, J. T.; et al. *Nat. Nanotechnol.* **2012**, *7*, 180–184.
- (9) Hai, A.; Shappir, J.; Spira, M. E. *J. Neurophysiol.* **2010**, *104*, 559–568.
- (10) Tian, B.; et al. *Science* **2010**, *329*, 830–834.
- (11) Jiang, Z.; Qing, Q.; Xie, P.; Gao, R.; Lieber, C. M. *Nano Lett.* **2012**, *12*, 1711–1716.
- (12) Duan, X.; et al. *Nat. Nanotechnol.* **2012**, *7*, 174–179.
- (13) Gao, R.; et al. *Nano Lett.* **2012**, *12*, 3329–3333.
- (14) Qing, Q.; Jiang, Z.; Xu, L.; Gao, R.; Mai, L.; Lieber, C. M. *Nat. Nanotechnol.* **2014**, *9*, 142–147.
- (15) Xu, L.; et al. *Nano Lett.* **2013**, *13*, 746–751.

(16) We consider $\pm 30^\circ$ deviation from the designated direction of the predefined probe body as acceptable because it can be later compensated by adjusting the slope of the micromanipulator. For a randomly oriented population of nanowires, this gives a yield of $60/360 \approx 17\%$.

(17) Buzsaki, G. *Nat. Neurosci.* **2004**, *7*, 446–451.

(18) Tian, B.; Xie, P.; Kempa, T. J.; Bell, D. C.; Lieber, C. M. *Nat. Nanotechnol.* **2009**, *4*, 824–829.

(19) See Supporting Information

(20) Yao, J.; Yan, H.; Lieber, C. M. *Nat. Nanotechnol.* **2013**, *8*, 329–335.

(21) Yu, G.; Lieber, C. M. *Pure Appl. Chem.* **2010**, *82*, 2295–2314.

(22) Li, B.; Liu, M.; Chen, Q. *J. Micro/Nanolith. MEMS MOEMS* **2005**, *4* (4), 043008.

(23) Bers, D. M. *Nature* **2002**, *415*, 198–205.

(24) Zipes, D. P.; Jalife, J. *Cardiac Electrophysiology: From Cell to Bedside*, 2nd ed.; Saunders: Philadelphia, 2009.